Received September 2, 2020, accepted September 15, 2020, date of publication September 21, 2020,
date of current version September 29, 2020.

Digital Object Identifier 10.1109/ACCESS.2020.3025291

A Novel h–φ Approach for Solving Eddy–Current Problems in Multiply Connected Regions

FEDERICO MORO[1], (Member, IEEE), JASMIN SMAJIC[2], (Senior Member, IEEE), AND LORENZO CODECASA[3], (Member, IEEE)

[1]Dipartimento di Ingegneria Industriale, Università degli Studi di Padova, 35131 Padova, Italy
[2]Institute of Electromagnetic Fields, Swiss Federal Institute of Technology (ETH Zürich), 8092 Zürich, Switzerland
[3]Dipartimento di Elettronica, Informazione e Bioingegneria, Politecnico di Milano, 20133 Milano, Italy

Corresponding author: Federico Moro (federico.moro@unipd.it)

ABSTRACT A novel **h**–φ approach for solving 3–D time–harmonic eddy current problems is presented. It makes it possible to limit the number of degrees of freedom required for the discretization such as the **T**–Ω method, while overcoming topological issues related to it when multiply connected domains are considered. Global basis functions, needed for representing magnetic field in the insulating region, are obtained by a fast iterative solver. The computation of thick cuts by high–complexity computational topology tools, typically required by the **T**–Ω method, is thus avoided. The final matrix system turns out to be symmetric and full–rank unlike the more classical **A**–**A** method, which requires gauging of magnetic vector potential to ensure uniqueness. Numerical tests show that the proposed method is accurate and the field problem solution is obtained in a reasonable computational time even for 3–D models with millions of mesh elements.

INDEX TERMS Eddy currents, finite element method, cell method, multiply connected, cut.

I. INTRODUCTION

The **T**–Ω method is known to be one of the most efficient methods for eddy–current problems because, by using nodal unknowns (i.e., the scalar potential Ω) in the insulating domain and restricting the support of electric vector potential **T** to conducing regions only, greatly limits the number of degrees of freedom (DOFs) required for the discretization compared to other eddy–current formulations [1], [2]. With multiply connected domains, the **T**–Ω method requires, however, to build the so–called *thick cuts*, i.e., layers of tetrahedral cells filling conductor holes, in order to impose the curl–free condition of **T** without violating Ampère's law and, at the same time, to make Ω single–valued in the insulating region [3]. Basis functions, i.e., *generators*, required for representing curl–free fields that are not gradients, i.e., the *first de Rham cohomology group*, have their support on thick cuts. The construction of thick cuts implies the identification of *cutting surfaces*, to which mesh elements of the thick cut are attached [4], [5]. This identification procedure is known to be a non–trivial task and a number of different strategies have been proposed in the literature over more than thirty years of research. Most of them rely on homology computations based on modular arithmetic (with super-cubic complexity) [6], [7], or constrained spanning–tree algorithms (typically problem dependent) [8]–[10]. More recently, an algorithm for computing generators directly at the cohomology level has been proposed in [11]. Even though it allows greatly reducing computational time with respect to previous techniques, extracted generators are not linearly independent since their number is twice the dimension of de Rham group.

In order to avoid main drawbacks of previous approaches, a decomposition of the magnetic field in terms of a scalar potential, which does not make use of cuts, is here adopted. In order to extract cohomology generators needed for this decomposition, a novel algorithm—operating directly at the algebraic level—is proposed. Such an algorithm does not make use of operations based on modular arithmetic and it is not problem dependent. Moreover, a maximal set of generators is obtained so that matrix fill–in and conditioning worsening are limited. The key idea of this algebraic algorithm is to compute cohomology generators by solving matrix systems, obtained from the discretization of topological equations, by using iterative solvers with limited computational cost. This approach extends that one already developed for finding topological bases useful to enforce non–local

The associate editor coordinating the review of this manuscript and approving it for publication was Muhammad Zubair.

constraints on magnetic field sources such as AC current– or voltage–driven coils [25]. The algebraic algorithm here proposed is used for implementing an eddy–current formulation using a reduced magnetic scalar potential φ in the insulating domain and the magnetic field $\mathbf{H}$ in the conducting parts. Note that other choices, equally based on a scalar potential, such as $\mathbf{T}$–Ω or $\mathbf{A}$–φ, are also possible and will be investigated elsewhere.

The $\mathbf{H}$–φ method was originally proposed as a magnetic formulation, alternative to the ''electric'' one based on the magnetic vector potential $\mathbf{A}$ [13], [14]. Even though the $\mathbf{H}$–φ method is well–assessed for eddy–current problems with simply connected domains [15], [16], only a few works in the literature deal with the multiply connected case [17]–[20].

The eddy–current problem is here discretized by using the Cell Method (CM), in which partial differential equations are expressed directly in algebraic form, amenable to numerical computation [21]. Problem variables of CM formulations are arrays of DOFs, whose coefficients are scalar potentials or integrals related to geometric entities like edges, faces, or cells of the computational domain mesh. The discretization process resembles that one of electric network theory, in which topological equations (i.e., Kirchhoff's laws) are split from constitutive equations (e.g., Ohm's law), and eventually these are assembled together for yielding the final matrix system. The CM variant proposed in [22] is here adopted because, by introducing *augmented dual grids*, it fixes some limitations of the original CM in [21] (e.g., not enforcing properly energy conservation) and introduces new discrete operators for handling either boundary or interface conditions. These peculiar features of this CM variant are key ingredients for building the numerical method here proposed.

The CM has already been adopted for the discretization of 3–D time–harmonic eddy–current problems formulated in terms of edge DOFs, i.e., line integrals of $\mathbf{A}$ [23], [24]. This electric formulation has been extended in [25] to multiply connected problems with an unbounded air domain by hybridization with the boundary element method (BEM). In this work, the eddy–current problem is discretized by using the CM in the whole computational domain and it is formulated in terms of magnetic edge variables $\mathbf{h}$, i.e., line integrals of $\mathbf{H}$ in conducting regions, and nodal variables $\boldsymbol{\varphi}$, i.e., scalar potentials in insulating region. Additional unknowns $\boldsymbol{\xi}$, i.e., DOFs related to cohomology generators, are needed for introducing $\boldsymbol{\varphi}$ in the multiply connected insulating domain.

The paper is organized as follows. The eddy–current problem setting and its topological features are first examined in Section II, where the decomposition of $\mathbf{H}$ is presented. The CM discretization framework, with augmented dual grid, is described in Section III. Section IV is dedicated to the discussion of algorithm for constructing the cohomology basis, which is one of the major contributions of this work. The CM formulation is presented in Section V, where details about the source field (for simulating AC current–driven coils), the magnetic scalar potential formulation in the insulating domain, and the discrete diffusion equation in conducting parts are provided. Interface conditions and the solution procedure, yielding a full–rank complex symmetric system amenable to iterative solution, are finally described. The last part of the paper deals with numerical results. Two benchmarks are presented in Section VI. The first one consists in an axisymmetric problem, solved by third–order 2–D FEM in order to get highly accurate results for comparisons. The second one is the Team Problem 3 ''Bath Plate'', which makes it possible to test the $\mathbf{h}$–$\boldsymbol{\varphi}$ method on a real-sized 3–D model.

II. TOPOLOGICAL PRELIMINARIES

The eddy–current field problem is defined in a computational domain Ω, which is assumed to be an open and bounded subset of $\mathbb{R}^3$, made of a multiply connected conducting subdomain Ω_C, such that $\overline{\Omega}_C \subseteq \Omega$, where the bar notation indicates the set closure, and an insulating subdomain $\Omega_I = \Omega \setminus \overline{\Omega}_C$ (Fig. 1). Note that both Ω_C and Ω_I can be made up of several non–connected components and Ω_C does not intersect the domain boundary $\partial\Omega$, such that $\partial\Omega_C \cap \partial\Omega = \emptyset$.

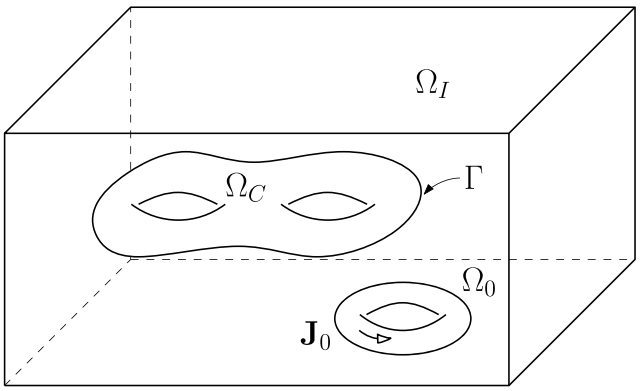

FIGURE 1. Computational domain for the eddy current problem: Ω_C is the multiply connected conducting subdomain, Ω_I the insulating subdomain, and Ω_0 source subdomain with current density $\mathbf{J}_0$; Γ separates Ω_C and Ω_I.

The domain Ω_C contains conducting media (with locally piecewise uniform resistivity ρ). Ω_I, which may be disconnected as well (e.g., cavities filled of air inside Ω_C) is made of magnetic media (insulating, with locally piecewise uniform permeability μ). The boundaries of Ω_C and Ω_I are indicated, respectively, as $\partial\Omega_C$ and $\partial\Omega_I$, which are oriented by their respective outward unit normal vectors $\mathbf{n}_{\partial\Omega_C}$, $\mathbf{n}_{\partial\Omega_I}$. The interface between these subdomains is defined to be $\Gamma = \overline{\partial\Omega}_C \cap \overline{\partial\Omega}_I$. The traces of the subdomain boundaries on Γ are defined as $\Gamma_C = \partial\Omega_C \cap \Gamma$ and $\Gamma_I = \partial\Omega_I \cap \Gamma$, each one carrying the corresponding subdomain orientation. Noting that $\overline{\Omega}_C \subseteq \Omega$ and $\partial\Omega_C \cap \partial\Omega = \emptyset$, it results $\Gamma = \Gamma_C$. The interface is assumed to be oriented such as Γ_C, so that its unit normal vector becomes $\mathbf{n}_\Gamma = \mathbf{n}_{\Gamma_C}$. Note also that $\mathbf{n}_{\Gamma_I} = -\mathbf{n}_\Gamma$ and $\partial\Omega_I = \Gamma_I \cup \partial\Omega$. Magnetic field sources are AC current–driven coils operating at constant frequency. They are represented by the subdomain $\Omega_0 \subseteq \Omega_I$, where a source current density $\mathbf{J}_0$ is impressed. Note that Ω_0 is strictly

embedded in the insulating region, such that $\partial\Omega_0 \cap \partial\Omega_I = \emptyset$. In the following, time–harmonic field problem (scalar or vector) variables are represented in the frequency domain as complex phasors.

In order to avoid cuts for the definition of scalar potential in the multiply connected domain, it is very well–known in the literature that this decomposition of the magnetic field can be adopted in the insulating domain [8], [25], [27]:

$$\mathbf{H} = \mathbf{H}_s - \nabla\varphi_r + \sum_{k=1}^{\beta_1} I_k \, \mathbf{H}_k, \tag{1}$$

where $\mathbf{H}_s$ is the magnetic field computed by Biot-Savart's integral from $\mathbf{J}_0$, φ_r is the reduced scalar potential, and $\mathbf{H}_k$, $k = 1, \ldots, \beta_1$, with β_1 first Betti number of Ω_I, are magnetic fields generated by equivalent coils (strictly embedded into Ω_C), each one carrying a current I_k. These equivalent loops are required in order to properly enforce Ampère's law on conductors. The main inconvenient is that these topological fields require the introduction of cuts Σ_k across Ω_C, such that, for any $k = 1, \ldots, \beta_1$, $\int_{\partial\Sigma_j} \mathbf{H}_k \cdot d\mathbf{l} = \delta_{kj}$ holds.

In order to avoid this drawback, the following decomposition, which does not make use of currents as DOFs and it is merely mathematical, is here adopted [18], [26]:

$$\mathbf{H} = \mathbf{H}_0 + \nabla\varphi + \sum_{k=1}^{\beta_1} \xi_k \, \mathbf{T}_k, \tag{2}$$

where the *source field* $\mathbf{H}_0$ is *any field* such that $\nabla\times\mathbf{H}_0 = \mathbf{J}_0$, φ is a generic scalar potential, and ξ_k are complex coefficients, which are not currents through cuts. In such a way, *loop fields* $\mathbf{T}_k$ do not enforce Ampère's law on conductors and are linear combinations of previously defined $\mathbf{H}_k$. These loop fields form a basis of curl–free fields in Ω_I that are not gradient of any scalar field, i.e., a *first de Rham cohomology group*. The algorithm for finding $\mathbf{T}_k$, proposed in [26], involves the computation of linking numbers and the preliminary construction of a homology basis of Ω_I, which implies in turn a reduction procedure and the computation of a Smith Normal Form (SNF). These constructions imply, however, high computational costs, i.e., linking numbers are computed from double line integrals with quadratic cost, whereas SNF algorithms typically exhibit a super–cubic complexity [7].

The key idea of this work is to avoid instead these preliminary constructions by means of the algorithm proposed in Section IV, which makes it possible to construct the field loop basis directly at the algebraic level by using an iterative solver for rectangular matrix systems, such as LSMR or LSQR, and orthogonalization, such as a QR algorithm with update.

In order to determine ξ_k, $k = 1, \ldots, \beta_1$, suitable topological constraints are required. Following the same approach as [25] (Section IV.B), these are obtained from the *virtual energy conservation principle* applied to Ω_I, that is

$$\int_{\Omega_I} \mathbf{B}' \cdot \mathbf{H} \, d\Omega + \int_{\Omega_I} \mathbf{A}' \times \mathbf{H} \cdot \mathbf{n}_{\Gamma_I} d\Gamma = \int_{\Omega_I} \mathbf{A}' \cdot \mathbf{J}_0 \, d\Omega, \tag{3}$$

where $\mathbf{A}'$, $\mathbf{B}'$ are arbitrary vector fields. It is shown in [25] that the following constraints can be obtained from (3):

$$\int_{\Omega_I} \mathbf{T}_k \cdot (\mathbf{B} - \nabla\times\mathbf{A}) \, d\Omega = 0, \quad k = 1, \ldots, \beta_1. \tag{4}$$

where $\mathbf{B}$ is the magnetic flux density. From Faraday's law, it results $\nabla\times\mathbf{A} = -(\jmath\omega)^{-1}\nabla\times\mathbf{E}$, with $\jmath$ imaginary unit, ω angular frequency, and $\mathbf{E}$ electric field. Integrating by parts and noting that any field $\mathbf{T}_k$ is curl–free, topological constraints (4) become for any $k = 1, \ldots, \beta_1$:

$$\jmath\,\omega \int_{\Omega_I} \mathbf{T}_k \cdot \mathbf{B} \, d\Omega + \int_{\partial\Omega_I} \mathbf{E} \times \mathbf{T}_k \cdot \mathbf{n}_{\partial\Omega_I} \, d\Gamma = 0, \tag{5}$$

where the surface integral includes also the contribution from domain boundary. By assuming homogeneous Dirichlet BCs, $\mathbf{n}_{\partial\Omega} \times \mathbf{E} = \mathbf{0}$ on $\partial\Omega$, i.e., no magnetic flux though the domain boundary, as typically done for time–harmonic eddy–current problems with an air region (see, e.g., [3]), topological constraints can be finally recast for any $k = 1, \ldots, \beta_1$, as:

$$\jmath\,\omega \int_{\Omega_I} \mathbf{T}_k \cdot \mathbf{B} \, d\Omega + \int_{\Gamma_I} \mathbf{T}_k \cdot \mathbf{n}_{\Gamma_I} \times \mathbf{E} \, d\Gamma = 0. \tag{6}$$

III. CELL METHOD WITH AUGMENTED DUAL GRID

The eddy–current problem is discretized according to the CM, as follows. The computational domain is meshed into tetrahedral elements. Any subdomain $\Omega_i \subseteq \Omega$, $i \in \{C, I, 0\}$, is discretized by its mesh partition $\mathcal{G}_{\Omega_i}$, i.e., the so–called *primal grid*, made up of N_{Ω_i} vertexes, E_{Ω_i} edges, F_{Ω_i} faces, and V_{Ω_i} cells. The *boundary primal grid* $\mathcal{G}_{\partial\Omega_i}$ is the restriction of $\mathcal{G}_{\Omega_i}$ to its boundary $\partial\Omega_i$, in which vertexes are traces of bulk primal edges of $\mathcal{G}_{\Omega_i}$), edges are traces of bulk primal faces, and faces are traces of bulk primal volumes. $\mathcal{G}_{\Omega_i}$ and $\mathcal{G}_{\partial\Omega_i}$ are then split into their corresponding barycentric subdivisions, which are obtained by splitting any tetrahedron or triangle into a set of tetrahedrons or triangles having as a common apex the cell centroid. The corresponding *domain dual grid* $\widetilde{\mathcal{G}}_{\Omega_i}$ (made of $\widetilde{N}_{\Omega_i}$ vertexes, $\widetilde{E}_{\Omega_i}$ edges, $\widetilde{F}_{\Omega_i}$ faces, and $\widetilde{V}_{\Omega_i}$ volumes) and *boundary dual grid* $\widetilde{\mathcal{G}}_{\partial\Omega_i}$ are finally obtained by joining barycentric cells (tetrahedrons for Ω_i or triangles for $\partial\Omega_i$). The *augmented dual grid* is the union of dual domain and boundary grids, that is $\widetilde{\mathcal{G}}_{\Omega_i\partial\Omega_i} = \widetilde{\mathcal{G}}_{\Omega_i} \cup \widetilde{\mathcal{G}}_{\partial\Omega_i}$ according to [22]. This specific geometric construction provides a one–to–one correspondence between primal and dual grid entities so that $\widetilde{N}_{\Omega_i} = V_{\Omega_i}$, $\widetilde{E}_{\Omega_i} = F_{\Omega_i}$, $\widetilde{F}_{\Omega_i} = E_{\Omega_i}$, and $\widetilde{V}_{\Omega_i} = N_{\Omega_i}$. Similar relationships hold for the boundary grids. Note that in the case of the interface Γ, primal and dual grids are inherited from that ones of the boundary Γ_C, so that relationships $\mathcal{G}_\Gamma = \mathcal{G}_{\Gamma_C}$ and $\widetilde{\mathcal{G}}_\Gamma = \widetilde{\mathcal{G}}_{\Gamma_C}$ hold.

A sketch of this geometric construction is shown in Fig. 2, considering a 2–D mesh for the sake of simplicity. The augmented dual grid in Fig. 2c, discretizing a unit square $\Omega = [0, 1]^2$, is obtained from the primal grid (Fig. 2a) by assembling triangles of the barycentric subdivision (Fig. 2b). $\mathcal{G}_\Omega$, whose nodes are indicated by black dots in Fig. 2a, is made up of triangles (shaded in gray). The corresponding barycentric subdivision is built by taking as mesh vertexes

(blue dots) primal nodes and centroids of primal edges and cells. $\widetilde{\mathcal{G}}_\Omega$ is obtained by aggregating barycentric triangles around any primal node in order to get a one–to–one correspondence between primal nodes (black dots) and dual cells (polygon shaded in red). Dual nodes, which are centroids of primal cells and centroids of boundary edges, are indicated by red squares in Fig. 2c. In the same way, on the domain boundary (dashed line), $\widetilde{\mathcal{G}}_{\partial\Omega}$, made up of 1–D dual cells (red thick line in Fig. 2c), is constructed by joining barycentric cells (blue thick line in Fig. 2b). Note that, the other way round, a one–to–one correspondence also exists between dual nodes and primal cells, which can be either primal cells of $\mathcal{G}_\Omega$ or boundary edges of $\mathcal{G}_{\partial\Omega}$. Finally, the augmented dual grid is the union of bulk and boundary dual grids, i.e., $\widetilde{\mathcal{G}}_{\Omega\partial\Omega} = \widetilde{\mathcal{G}}_\Omega \cup \widetilde{\mathcal{G}}_{\partial\Omega}$.

Primal and dual cell complexes carry a different orientation according to [21]. Geometric entities of any $\mathcal{G}_{\Omega_i}$ are endowed by an *inner* orientation so that any vertex is oriented as a sink—i.e., any edge incident to that vertex is pointing inward—, any edge is oriented by a transversing direction (from one end to the other), any face is oriented clockwise or counterclockwise, and any cell is oriented by assuming that its facets are oriented counterclockwise with respect to the corresponding exterior normals. Similar considerations hold for the boundary mesh $\mathcal{G}_{\partial\Omega_i}$. Geometric entities of $\widetilde{\mathcal{G}}_{\Omega_i\partial\Omega_i}$ are endowed with *outer* orientation, which is inherited from that one of primal grid entities by one–to–one correspondence. In such a way, e.g., a dual edge is oriented by the same orientation of its corresponding primal face, i.e., a clockwise or counterclockwise rotation around it.

After assigning orientations, incidence matrices with integer coefficients $\{0, \pm 1\}$, discrete counterparts of gradient, divergence, curl differential operators, can be defined on dual grids. This can be regarded as a direct consequence of Stokes' theorem [28], [29]. Field problem variables in the CM are vectors of DOFs, i.e., nodal potentials, line, surface (fluxes), or volume integrals, whose sign convention is related the corresponding geometric entity orientation. It is assumed from now on that any vector of DOFs, indicated in lowercase bold font, is a column vector.

IV. ALGORITHM FOR THE COHOMOLOGY BASIS

By integrating (2) along primal edges of $\mathcal{G}_{\Gamma_I}$, one obtains:

$$\mathbf{h}_{\Omega_I} = \mathbf{h}_{0,\Omega_I} + \mathbf{G}_{\Omega_I}\,\boldsymbol{\varphi}_{\Omega_I} + \sum_{k=1}^{\beta_1} \xi_k\,\mathbf{t}_{\Omega_I,k} \tag{7}$$

where $\mathbf{h}_{\Omega_I} = (h_i)$ is the vector of magnetic voltages of $\mathcal{G}_{\Omega_I}$—i.e, line integrals of $\mathbf{H}$ along primal edges of $\mathcal{G}_{\Omega_I}$, with $h_i = \int_{e_i} \mathbf{H}\cdot d\mathbf{e}$—, and $\mathbf{G}_{\Omega_I}$ is the edges-to-nodes incidence matrix of $\mathcal{G}_{\Omega_I}$. In the same way, vectors $\mathbf{h}_{0,\Omega_I}$ and $\mathbf{t}_{\Omega_I,k}$, with $k = 1,\ldots,\beta_1$, corresponds to $\mathbf{H}_0$ and $\mathbf{T}_k$ in (2), and their coefficients are line integrals along primal edges of $\mathcal{G}_{\Omega_I}$. The *discrete source field* $\mathbf{h}_{0,\Omega_I}$ is obtained directly at the algebraic level as described in Section V-A. The vector $\boldsymbol{\varphi}_{\Omega_I} = (\varphi_i)$ is made up by coefficients φ_i that are potentials evaluated in primal nodes of $\mathcal{G}_{\Omega_I}$. Basis vectors in (7) can be conveniently grouped column-wise into a unique *topological matrix*:

$$\mathbf{T}_{\Omega_I} = \left[\mathbf{t}_{\Omega_I,1},\ldots,\mathbf{t}_{\Omega_I,\beta_1}\right]. \tag{8}$$

The procedure for finding the cohomology basis relies on the fact that the basis dimension is finite and it is equal to the first Betti number of Ω_I, β_1 [28]. It can be proven, from algebraic topology arguments, that $\beta_1 = g$, where g is the surface genus of the interface Γ [26]. In fact, homology generators of Γ include both generators of Ω_C and its complement Ω_I, which are in the same number as stated by Alexander duality. The genus can be computed as $g = p - \chi/2$, where p is the number of connected components of Γ and the Euler–Poincaré characteristic of $\mathcal{G}_\Gamma$ is defined as:

$$\chi = N_\Gamma - E_\Gamma + T_\Gamma, \tag{9}$$

where N_Γ, E_Γ, and T_Γ are, respectively, the number of vertexes, edges, and triangles of the interface mesh $\mathcal{G}_\Gamma$.

The key idea is now to observe that $\mathbf{t}_{\Omega_I,k}$ are curl–free fields that lie in the orthogonal complement of the image of $\mathbf{G}_{\Omega_I}$. This can be proven by the following arguments:

1) The discrete source field fulfills (17), so that its complement with respect to magnetic voltages $\mathbf{u}_{\Omega_I} = \mathbf{h}_{\Omega_I} - \mathbf{h}_{0,\Omega_I}$ is curl–free, that is:
$$\mathbf{C}_{\Omega_I}\mathbf{u}_{\Omega_I} = \mathbf{0}, \tag{10}$$
with $\mathbf{C}_{\Omega_I}$ faces-to-edges incidence matrix of $\mathcal{G}_{\Omega_I}$.
2) Because the identity $\mathbf{C}_{\Omega_I}\mathbf{G}_{\Omega_I} = \mathbf{0}$ holds, the solution space of matrix system (10), i.e., $V = \ker(\mathbf{C}_{\Omega_I})$, splits as a direct sum $V = W \oplus W^\perp$, where $W = \mathrm{im}(\mathbf{G}_{\Omega_I})$ and $W^\perp$ is the corresponding orthogonal complement with respect to an inner product. Finally, from the first isomorphism theorem, it results $V/W \cong W^\perp$, where the quotient space V/W is spanned by the co-sets related to loop fields, i.e., $[\mathbf{t}_{\Omega_I,k}]$, $k = 1,\ldots,\beta_1$.

Therefore, in order to find loop fields, one may extract a basis from the solutions of (10) by means of a Gram-Schmidt orthogonalization procedure. At this purpose, the following inner product is defined in Ω_I:

$$(\mathbf{X},\mathbf{Y})_\mu = \int_{\Omega_I} \mathbf{X}\cdot\mu\,\mathbf{Y}\,d\Omega, \tag{11}$$

for any pair vector fields $\mathbf{X},\mathbf{Y} \in \left(L^2(\Omega_I)\right)^3$. By expanding these vector fields by means of piecewise edge basis functions $\mathbf{w}_{e_i}$ and resorting again to their consistency property, the following discrete inner product is induced in $\mathbb{R}^n$:

$$(\mathbf{x}_{\Omega_I},\mathbf{y}_{\Omega_I})_\mu = \mathbf{x}_{\Omega_I}^{\mathrm{T}}\mathbf{M}_{\mu,\Omega_I}\mathbf{y}_{\Omega_I}, \tag{12}$$

where $\mathbf{M}_{\mu,\Omega_I}$ is the magnetic constitutive matrix of $\mathcal{G}_{\Omega_I}$ (see Section V-C), $(\cdot)^{\mathrm{T}}$ indicates the transpose of a vector or a matrix, and $\mathbf{x}_{\Omega_I} = (x_i)$, $\mathbf{y}_{\Omega_I} = (y_i)$ are vectors of DOFs, whose coefficients $x_i = \int_{e_i}\mathbf{X}\cdot d\mathbf{e}$, $y_i = \int_{e_i}\mathbf{Y}\cdot d\mathbf{e}$ are line integrals along primal edges e_i of $\mathcal{G}_{\Omega_I}$. The inner product (12) induces, on its turn, the *energy norm* $\|\mathbf{x}_{\Omega_I}\|_\mu = \sqrt{(\mathbf{x}_{\Omega_I},\mathbf{x}_{\Omega_I})_\mu}$.

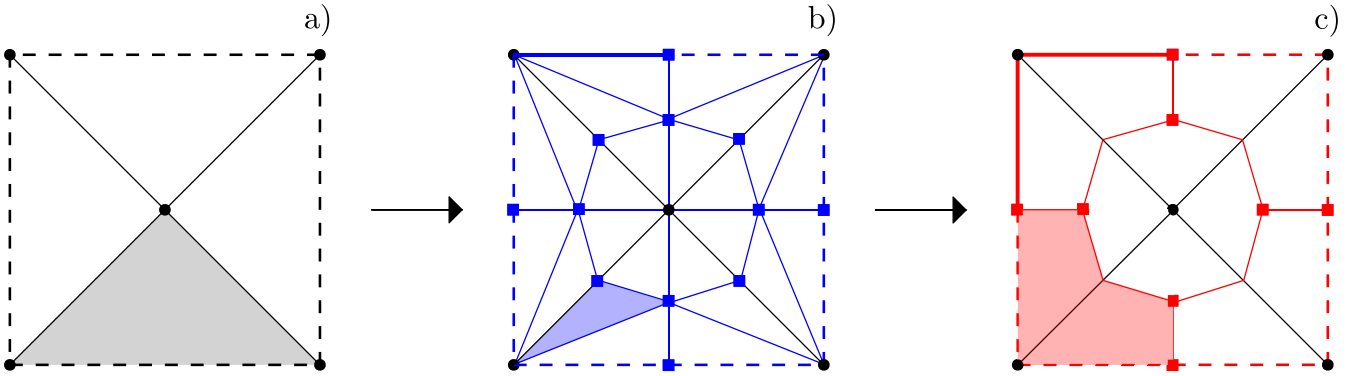

FIGURE 2. Example for a 2–D mesh discretizing $\Omega = [0, 1]^2$: (a) Primal grid $\mathcal{G}_\Omega$; (b) Barycentric subdivision; (c) Augmented dual grid $\tilde{\mathcal{G}}_{\Omega\partial\Omega}$. The augmented dual grid is obtained from the barycentric subdivision by aggregating triangles in blue around any primal node. A one-to-one correspondence exists between primal nodes (black dots) and dual cells (polygon in red), and between dual nodes (red dots) and primal cells (triangle in gray). Note that the boundary (dashed line) is split on its turn into barycentric cells (blue thick line),which are joined into 1–D dual cells (red thick line).

Algorithm 1 Discrete Cohomology Basis

1: $\mathbf{T}_{\Omega_I} := []$
2: Find connected components $\mathcal{G}_\Gamma^{(m)}$ of $\mathcal{G}_\Gamma$
3: Init the number of generators $k := 0$
4: Init the interface genus $g := 0$
5: **for** $m = 1, \ldots, M$ **do**
6: $\quad \chi_m := N_\Gamma^{(m)} - E_\Gamma^{(m)} + T_\Gamma^{(m)}$
7: $\quad$ Component genus $g_m := 1 - \chi_m/2$
8: $\quad g := g + g_m$
9: $\quad$ Init set $\mathcal{E}_\Gamma^{(m)}$ of edges of $\mathcal{G}_\Gamma^{(m)}$
10: $\quad$ **if** $g_m > 0$ **then**
11: $\quad\quad$ **while** $k < g$ **do**
12: $\quad\quad\quad$ Pick at random the j–th edge of $\mathcal{E}_\Gamma^{(m)}$
13: $\quad\quad\quad$ Solve (10) for $\mathbf{u}_{\Omega_I}$, setting $\mathbf{u}_{\Omega_I,j} = 1$
14: $\quad\quad\quad$ Compute the orthogonal complement $\mathbf{v}_{\Omega_I}$ of $\mathbf{u}_{\Omega_I}$ with respect to the image of $\mathbf{G}_{\Omega_I}$
15: $\quad\quad\quad$ Compute the orthogonal complement $\mathbf{w}_{\Omega_I}$ of $\mathbf{v}_{\Omega_I}$ with respect to the image of $\mathbf{T}_{\Omega_I}$
16: $\quad\quad\quad$ **if** $\|\mathbf{w}_{\Omega_I}\|_\mu > 0$ **then**
17: $\quad\quad\quad\quad k := k + 1$
18: $\quad\quad\quad\quad \mathbf{t}_{\Omega_I,k} := \mathbf{w}_{\Omega_I}/\|\mathbf{w}_{\Omega_I}\|_\mu$
19: $\quad\quad\quad\quad \mathbf{T}_{\Omega_I} := \left[\mathbf{T}_{\Omega_I}, \mathbf{t}_{\Omega_I,k}\right]$
20: $\quad\quad\quad$ **end if**
21: $\quad\quad$ **end while**
22: $\quad$ **end if**
23: **end for**

The procedure for finding the discrete cohomology basis is summarized in the Algorithm 1.

At line 1, the set of cohomology generators (indicated as the topological matrix) $\mathbf{T}_{\Omega_I}$ is initialized to an empty set.

At line 2, the connected components $\mathcal{G}_\Gamma^{(m)}$ of the primal grid $\mathcal{G}_\Gamma$, such that $\mathcal{G}_\Gamma = \bigcup_{m=1}^{M} \mathcal{G}_\Gamma^{(m)}$, are identified.

At lines 6, 7, for any component $m = 1, \ldots, M$, the genus g_m of $\mathcal{G}_\Gamma^{(m)}$ is computed from its Euler's characteristic χ_m. Cohomology generators are found after testing, at line 10, that the topology is non–trivial, i.e., $g_m > 0$.

At line 13, an admissible curl–free field $\mathbf{u}_{\Omega_I} = (u_k)$ is found by solving (10) with LSMR or, equivalently LSQR. In order to obtain a non–trivial solution one DOF, related the j–th, randomly chosen edge of $\mathcal{G}_\Gamma^{(m)}$, is set to one, i.e., $u_j = 1$.

At line 14, the orthogonal complement $\mathbf{v}_{\Omega_I}$ of $\mathbf{u}_{\Omega_I}$ with respect to the image of $\mathbf{G}_{\Omega_I}$ is found by setting:

$$(\mathbf{g}_n, \mathbf{v}_{\Omega_I,k})_\mu = 0, \quad n = 1, \ldots, N_{\Omega_I}, \tag{13}$$

where $\mathbf{g}_n$ is the n–th column of $\mathbf{G}_{\Omega_I}$. These can be recast in matrix form by letting $\mathbf{v}_{\Omega_I} = \mathbf{u}_{\Omega_I} - \mathbf{G}_{\Omega_I}\boldsymbol{\varphi}_{\Omega_I}$, as:

$$\mathbf{G}_{\Omega_I}^{\mathrm{T}}\mathbf{M}_{\mu,\Omega_I}\mathbf{G}_{\Omega_I}\,\boldsymbol{\varphi}_{\Omega_I} = \mathbf{G}_{\Omega_I}^{\mathrm{T}}\mathbf{M}_{\mu,\Omega_I}\mathbf{u}_{\Omega_I}. \tag{14}$$

Matrix system (14) can be solved by an efficient algebraic multigrid solver for elliptic field problems such as AGMG [35]. $\mathbf{v}_{\Omega_I}$ is obtained from the solution of (14) and from $\mathbf{u}_{\Omega_I}$, and it is finally normalized with respect to the energy norm.

At line 15, the orthogonal complement $\mathbf{w}_{\Omega_I}$ of $\mathbf{v}_{\Omega_I}$ is found with respect to subspace generated by vectors $\mathbf{t}_{\Omega_I,k}$ that have already been extracted.

At line 16, a linear dependency check of $\mathbf{w}_{\Omega_I}$ is realized. If its energy norm is non–trivial, then it is linearly independent with respect to previous generators. It is normalized at line 18 and added to the set of generators at line 19.

Iterations are stopped at line 11, when a number of g_m generators has been extracted for the component $\mathcal{G}_\Gamma^{(m)}$.

It is very important to note that any $\mathbf{w}_{\Omega_I}$ is obtained by using a QR decomposition with column update, avoiding the reorthonormalization from scratch which typically involves $\mathcal{O}(N^3)$ computational complexity [36]. It can be observed also that, since $\mathbf{t}_{\Omega_I,k} \in W^\perp$ for any $k = 1, \ldots, \beta_1$, the following orthogonality conditions hold:

$$(\mathbf{g}_n, \mathbf{t}_{\Omega_I,k})_\mu = 0, \quad n = 1, \ldots, N_{\Omega_I}, \tag{15}$$

which can be rewritten more compactly in matrix form as:

$$\mathbf{G}_{\Omega_I}^{\mathrm{T}}\mathbf{M}_{\Omega_I}\mathbf{T}_{\Omega_I} = \mathbf{0}. \tag{16}$$

V. CELL METHOD MAGNETIC FORMULATION

In the following the CM discretization process is specialized to any subdomain in order to obtain field problem equations directly in algebraic form, suitable for assembling the final matrix system of the **h**–$\boldsymbol{\varphi}$ approach.

A. SOURCE FIELD IN Ω_I

It is very well know in literature that the source field $\mathbf{H}_0$ in (2) should not necessarily be the solution of a magnetostatic problem, which requires the time–consuming computation of Biot-Savart's integrals [30], [31]. The only constraint to fulfill is the local Ampère law $\nabla\times\mathbf{H}_0=\mathbf{J}_0$, with boundary conditions $\mathbf{J}_0\cdot\mathbf{n}=0$ on $\partial\Omega_0$. In the framework of the CM, an admissible discrete source field is provided by the solution of the global Ampère law in the insulating domain, that is:

$$\mathbf{C}_{\Omega_I}\,\mathbf{h}_{0,\Omega_I}=\mathbf{j}_{0,\Omega_I}, \tag{17}$$

where $\mathbf{j}_{0,\Omega_I}=(j_{0,i})$ is the vector of source currents, where $j_{0,i}=\int_{f_i}\mathbf{J}_0\cdot d\mathbf{f}$ are fluxes through primal faces f_i of $\mathcal{G}_{\Omega_I}$. Note that these coefficients are zero for faces lying in $\Omega_I\setminus\Omega_0$. The source field is constructed directly at the algebraic level by using an iterative solver for solving rectangular systems, such as LSMR or LSQR. In such a way, it is not necessary to construct a tree-cotree decomposition and fundamental loops in order to identify independent DOFs, as proposed in [33].

The source current density in Ω_0 can be reconstructed after imposing the source current I_0 by using the algebraic approach proposed in [12]. In the case of coils with simple shape (e.g., circular coils), however, $\mathbf{J}_0$ is typically known a priori by analytical formulas. The procedure below adapts the approach in [12] to the case of analytical field sources.

For the sake of simplicity, a single coil is considered in Ω_0; however, the following procedure can be easily extended in the most general case of multiple sources. For a single coil, the source current density can be expanded as [12]:

$$\mathbf{J_0}=\nabla\times\mathbf{T}_0+I_0\,\mathbf{K}_0, \tag{18}$$

where $\mathbf{T}_0$ is the electric vector potential in Ω_0, under BCs $\mathbf{n}\times\mathbf{T}_0=\mathbf{0}$ on $\partial\Omega_0$, and $\mathbf{K}_0$ is any div–free field which is not a curl of any vector field, such that $\int_{\Sigma_0}\mathbf{K}_0\cdot\mathbf{n}\,d\Sigma=1$, where Σ_0 is any surface (cutting Ω_0) on which I_0 is enforced.

For discretizing (18) by means of the CM, the following incidence matrices are introduced: $\mathbf{D}_{\Omega_0}$ (volumes to faces of $\mathcal{G}_{\Omega_0}$), $\mathbf{C}_{\Omega_0}$ (faces to edges of $\mathcal{G}_{\Omega_0}$), $\widetilde{\mathbf{D}}_{\Omega_0}=-\mathbf{G}^{\mathrm{T}}_{\Omega_0}$ (volumes to faces of $\widetilde{\mathcal{G}}_{\Omega_0}$), $\widetilde{\mathbf{C}}_{\Omega_0}=\mathbf{C}^{\mathrm{T}}_{\Omega_0}$ (faces to edges of $\widetilde{\mathcal{G}}_{\Omega_0}$), and $\mathbf{D}_{\Sigma_0\Omega_0}$ (cut Σ_0 to the faces of $\mathcal{G}_{\Omega_0}$). The topological field $\mathbf{K}_0$ is efficiently obtained at the discrete level by solving the following rectangular system by using again the LSMR or, equivalently, the LSQR iterative solver:

$$\mathbf{D}_{\Omega_0}\,\mathbf{k}_{\Omega_0}=\mathbf{0}, \tag{19}$$

$$\mathbf{k}_{\partial\Omega_0}=\mathbf{0}, \tag{20}$$

$$\mathbf{D}_{\Sigma_0\Omega_0}\,\mathbf{k}_{\Omega_0}=1, \tag{21}$$

where $\mathbf{k}_{\Omega_0}=(k_{0,i})$ is the discrete topological field, with $k_{0,i}=\int_{f_i}\mathbf{K}_0\cdot d\mathbf{f}$ fluxes through primal faces f_i of $\mathcal{G}_{\Omega_0}$, and $\mathbf{k}_{\partial\Omega_0}$ is its restriction to boundary $\partial\Omega_0$. Note that $\mathbf{K}_0$, in the continuous setting, does not have to be explicitly computed.

By discretizing (18) with the CM a rectangular system to be solved by LSMR in $\mathbf{t}_0=(t_{0,i})$, with $t_{0,i}=\int_{e_i}\mathbf{T}_0\cdot d\mathbf{e}$ line integrals along the primal edges e_i of $\mathcal{G}_{\Omega_0}$, is obtained:

$$\mathbf{C}_{\Omega_0}\,\mathbf{t}_{0,\Omega_0}=\mathbf{j}^*_{0,\Omega_0}-I_0\,\mathbf{k}_{0,\Omega_0}, \tag{22}$$

$$\mathbf{t}_{0,\partial\Omega_0}=\mathbf{0}, \tag{23}$$

where $\mathbf{j}^*_{0,\Omega_0}=(j^*_{0,i})$ is the vector of source currents, with fluxes $j^*_{0,i}=\int_{f_i}\mathbf{J}_0\cdot d\mathbf{f}$ numerically computed, e.g., by a three-point Gaussian quadrature rule. $\mathbf{t}_{0,\Omega_0}$ and $\mathbf{k}_{\Omega_0}$ finally provide a div–free discrete field which lies (up to machine precision) in the range of discrete curl operator in (17), i.e.,

$$\mathbf{j}_{0,\Omega_0}=\mathbf{C}_{\Omega_0}\,\mathbf{t}_{0,\Omega_0}+I_0\,\mathbf{k}_{0,\Omega_0}. \tag{24}$$

On the contrary, source vector $\mathbf{j}^*_{0,i}$ in general does not ensure the div–free condition and the compatibility with curl operator, because of the numerical approximation in the integration. As noted in [32], non–compatibly may affect the convergence of iterative solvers when solving curl–curl systems arising in the discretization of eddy–current problems.

B. EDDY CURRENTS IN Ω_C

The time–harmonic diffusion within conductors is formulated in terms of magnetic field. For the CM discretization the following incidence matrices are required: $\mathbf{C}_{\Omega_C}$ (faces to edges of $\mathcal{G}_{\Omega_C}$), $\widetilde{\mathbf{C}}_{\Omega_C}=\mathbf{C}^{\mathrm{T}}_{\Omega_C}$ (faces to edges of $\widetilde{\mathcal{G}}_{\Omega_C}$), and $\widetilde{\mathbf{C}}_{\Omega_C\Gamma_C}$ (faces of $\widetilde{\mathcal{G}}_{\Omega_C}$ to edges of $\widetilde{\mathcal{G}}_{\Gamma_C}$). The diffusion equation is constructed starting from the Ampére's law in Ω_C, which written on the whole primal cell complex reads:

$$\mathbf{C}_{\Omega_C}\,\mathbf{h}_{\Omega_C}=\mathbf{j}_{\Omega_C}, \tag{25}$$

where $\mathbf{h}_{\Omega_C}=(h_i)$ is the vector of magnetic voltages, with $h_i=\int_{e_i}\mathbf{H}\cdot d\mathbf{e}$ line integrals along primal edges e_i of $\mathcal{G}_{\Omega_C}$, and $\mathbf{j}_{\Omega_C}=(j_i)$ is the vector of eddy currents, with $\mathbf{J}$ current density and $j_i=\int_{f_i}\mathbf{J}\cdot d\mathbf{f}$ fluxes through primal faces f_i of $\mathcal{G}_{\Omega_C}$. On the dual complex, the topological relationships is provided by the Faraday's law in phasor notation:

$$\widetilde{\mathbf{C}}_{\Omega_C}\widetilde{\mathbf{e}}_{\Omega_C}+\widetilde{\mathbf{C}}_{\Omega_C\Gamma_C}\widetilde{\mathbf{e}}_{\Gamma}=-\jmath\,\omega\,\widetilde{\mathbf{b}}_{\Omega_C}, \tag{26}$$

where $\jmath$ is the imaginary unit, ω is the angular frequency, $\widetilde{\mathbf{e}}_{\Omega_C}=(\widetilde{\mathcal{E}}_i)$ is the vector of electric voltages $\widetilde{\mathcal{E}}_i=\int_{\widetilde{e}_i}\mathbf{E}\cdot d\widetilde{\mathbf{e}}$ along dual edges $\widetilde{e}_i$ of $\widetilde{\mathcal{G}}_{\Omega_C}$, and $\widetilde{\mathbf{b}}_{\Omega_C}=(\widetilde{b}_i)$ is the vector of magnetic fluxes $\widetilde{b}_i=\int_{\widetilde{f}_i}\mathbf{B}\cdot d\widetilde{\mathbf{f}}$ fluxes through dual faces $\widetilde{f}_i$ of $\widetilde{\mathcal{G}}_{\Omega_C}$. Interface term $\widetilde{\mathbf{e}}_{\Gamma_C}$ allows for the coupling with Ω_I.

The behavior of magnetic and conducting media in Ω_C is described by local constitutive relationships, i.e., $\mathbf{B}=\mu\,\mathbf{H}$ and $\mathbf{E}=\rho\,\mathbf{J}$. The corresponding discrete constitutive relationships are obtained by expanding $\mathbf{H}$ and $\mathbf{J}$ with edge and face piecewise uniform basis functions $\mathbf{w}_{e_i}$ and $\mathbf{w}_{f_i}$, respectively, defined in [34] for tetrahedral meshes. The so–called *consistency property* of edge and face elements (see, e.g., [28]) allows DOFs of primal complex to be projected on the dual complex and plays a fundamental role in the construction of the discrete constitutive relationships within

the CM framework. By assuming locally uniform fields and exploiting the consistency property, one obtains:

$$\widetilde{b}_i = \int_{\Omega_C} \mathbf{w}_{e_i} \cdot \mu \mathbf{H}\, d\Omega = \sum_{k=1}^{E_{\Omega_C}} \int_{\Omega_C} \mu \mathbf{w}_{e_i} \cdot \mathbf{w}_{e_k}\, h_k\, d\Omega, \quad (27)$$

$$\widetilde{\mathcal{E}}_i = \int_{\Omega_C} \mathbf{w}_{f_i} \cdot \rho \mathbf{J}\, d\Omega = \sum_{k=1}^{F_{\Omega_C}} \int_{\Omega_C} \rho \mathbf{w}_{f_i} \cdot \mathbf{w}_{f_k}\, j_k\, d\Omega, \quad (28)$$

where E_{Ω_C} and F_{Ω_C} are the number of edges and faces of $\mathcal{G}_{\Omega_C}$, respectively. The latter can be cast in a matrix form as:

$$\widetilde{\mathbf{b}}_{\Omega_C} = \mathbf{M}_{\mu,\Omega_C} \mathbf{h}_{\Omega_C}, \quad (29)$$

$$\widetilde{\mathbf{e}}_{\Omega_C} = \mathbf{M}_{\rho,\Omega_C} \mathbf{j}_{\Omega_C}, \quad (30)$$

which represent the magnetic and the electric discrete constitutive relationship, respectively.

By letting constitutive relationships (29) and (30) in (26), and by using the discrete Ampère law (25) for eliminating currents, the discrete diffusion equation in $\mathcal{G}_{\Omega_C}$ is obtained:

$$\left(\mathbf{C}_{\Omega_C}^{\mathrm{T}} \mathbf{M}_{\rho,\Omega_C} \mathbf{C}_{\Omega_C} + \jmath\, \omega\, \mathbf{M}_{\mu,\Omega_C}\right) \mathbf{h}_{\Omega_C} + \widetilde{\mathbf{C}}_{\Omega_C \Gamma_C} \widetilde{\mathbf{e}}_{\Gamma_C} = \mathbf{0}. \quad (31)$$

C. MAGNETIC FIELD IN Ω_I

For the CM discretization of the magnetostatic problem in Ω_I these incidence matrices are required: $\widetilde{\mathbf{D}}_{\Omega_I} = -\mathbf{G}_{\Omega_I}^{\mathrm{T}}$ (volumes–to–faces of $\widetilde{\mathcal{G}}_{\Omega_I}$), $\widetilde{\mathbf{C}}_{\Omega_I \Gamma_I}$ (faces of $\widetilde{\mathcal{G}}_{\Omega_I}$ to edges of $\widetilde{\mathcal{G}}_{\Gamma_I}$), and $\widetilde{\mathbf{D}}_{\Omega_I \Gamma_I}$ (volumes of $\widetilde{\mathcal{G}}_{\Omega_I}$ to faces of $\widetilde{\mathcal{G}}_{\Gamma_I}$).

By assuming no magnetic flux through the domain boundary consistently with (6), when writing magnetic flux conservation for dual cells of $\widetilde{\mathcal{G}}_{\Gamma_I}$ one needs to consider only fluxes through dual faces of $\widetilde{\mathcal{G}}_{\Gamma_I}$, $\widetilde{\mathbf{b}}_{\Gamma_I}$. Therefore, Gauss's law applied to any dual cell of $\widetilde{\mathcal{G}}_{\Omega_I}$ is written in matrix form, as:

$$\widetilde{\mathbf{D}}_{\Omega_I} \widetilde{\mathbf{b}}_{\Omega_I} + \widetilde{\mathbf{D}}_{\Omega_I \Gamma_I} \widetilde{\mathbf{b}}_{\Gamma_I} = \mathbf{0}, \quad (32)$$

where $\widetilde{\mathbf{b}}_{\Omega_I} = (\widetilde{b}_i)$ is the vector of magnetic fluxes $\widetilde{b}_i = \int_{\widetilde{f}_i} \mathbf{B} \cdot d\widetilde{\mathbf{f}}$ through dual faces $\widetilde{f}_i$ of $\widetilde{\mathcal{G}}_{\Omega_I}$. Interface vector $\widetilde{\mathbf{b}}_{\Gamma_I}$ allows for the coupling with the interior problem in Ω_C.

Similarly to the eddy–current problem, the edge piecewise uniform bases can be used in order to construct the magnetic constitutive relationship in Ω_I:

$$\widetilde{\mathbf{b}}_{\Omega_I} = \mathbf{M}_{\mu,\Omega_I} \mathbf{h}_{\Omega_I}. \quad (33)$$

By letting (33) in (32) and by using (7), (32) becomes:

$$\mathbf{G}_{\Omega_I}^{\mathrm{T}} \mathbf{M}_{\mu,\Omega_I} \mathbf{G}_{\Omega_I} \boldsymbol{\varphi}_{\Omega_I} - \widetilde{\mathbf{D}}_{\Omega_I \Gamma_I} \widetilde{\mathbf{b}}_{\Gamma_I} = -\mathbf{G}_{\Omega_I}^{\mathrm{T}} \mathbf{M}_{\mu,\Omega_I} \mathbf{h}_{0,\Omega_I}. \quad (34)$$

Note that terms $\mathbf{G}_{\Omega_I}^{\mathrm{T}} \mathbf{M}_{\mu,\Omega_I} \mathbf{t}_{\Omega_I,k}$, stemming from (7), vanish for any $k = 1, \ldots, \beta_1$, due to orthogonality property (16).

Additional constraints for determining coefficient ξ_k are obtained from the discretization of (6). By expanding $\mathbf{T}_k$ with edge piecewise uniform bases and exploiting their consistency property, the first term in (6) can be rearranged as follows for any $k = 1, \ldots, \beta_1$:

$$\int_{\Omega_I} \mathbf{T}_k \cdot \mathbf{B}\, d\Omega = \sum_{i=1}^{E_{\Omega_I}} t_{k,i} \int_{\Omega_I} \mathbf{w}_{e_i} \cdot \mathbf{B}\, d\Omega = \sum_{i=1}^{E_{\Omega_I}} t_{k,i}\, \widetilde{b}_i = \mathbf{t}_{\Omega_I,k}^{\mathrm{T}} \widetilde{\mathbf{b}}_{\Omega_I}, \quad (35)$$

where E_{Ω_I} is the number of primal edges of $\mathcal{G}_{\Omega_I}$. By exploiting the consistency property of the so–called *twisted edge elements* $\mathbf{n}_\Gamma \times \mathbf{w}_{e_i}$, the second term in (6) becomes for any $k = 1, \ldots, \beta_1$:

$$\begin{aligned} \int_{\Gamma_I} \mathbf{T}_k \cdot \mathbf{n}_{\Gamma_I} \times \mathbf{E}\, d\Gamma &= \sum_{i=1}^{E_{\Omega_I}} t_{k,i} \int_{\Gamma_I} \mathbf{w}_{e_i} \cdot \mathbf{n}_{\Gamma_I} \times \mathbf{E}\, d\Gamma \\ &= -\sum_{i=1}^{E_{\Omega_I}} t_{k,i} \int_{\Gamma_I} \mathbf{E} \cdot \mathbf{n}_{\Gamma_I} \times \mathbf{w}_{e_i}\, d\Gamma \\ &= -\sum_{i=1}^{E_{\Omega_I}} t_{k,i}\, \widetilde{\mathcal{E}}_i = -\mathbf{t}_{\Gamma_I,k}^{\mathrm{T}} \widetilde{\mathbf{e}}_{\Gamma_I}. \end{aligned} \quad (36)$$

Interface terms in (36) are computed from bulk ones by means of selection matrices, i.e., $\mathbf{t}_{\Gamma_I,k} = \widetilde{\mathbf{C}}_{\Omega_I \Gamma_I}^{\mathrm{T}} \mathbf{t}_{\Omega_I,k}$. In fact, it has to be noted that the transpose of an incidence matrix—relating bulk to boundary geometric entities—is a selection matrix of interface terms [22]. By using the matrix definition (8) and with (35) and (36), topological constraints (6) can be finally recast in matrix form as:

$$\jmath\, \omega\, \mathbf{T}_{\Omega_I}^{\mathrm{T}} \widetilde{\mathbf{b}}_{\Omega_I} - \mathbf{T}_{\Omega_I}^{\mathrm{T}} \widetilde{\mathbf{C}}_{\Omega_I \Gamma_I} \widetilde{\mathbf{e}}_{\Gamma_I} = \mathbf{0}. \quad (37)$$

By letting (33) in (37) and by using (7), one obtains the discrete topological constraints in terms of $\mathbf{h}_{\Omega_I}$ and $\boldsymbol{\varphi}_{\Omega_I}$, as:

$$\jmath\, \omega\, \mathbf{T}_{\Omega_I}^{\mathrm{T}} \mathbf{M}_{\mu,\Omega_I} \mathbf{T}_{\Omega_I} \boldsymbol{\xi} - \mathbf{T}_{\Omega_I}^{\mathrm{T}} \widetilde{\mathbf{C}}_{\Omega_I \Gamma_I} \widetilde{\mathbf{e}}_{\Gamma_I} = -\jmath\, \omega\, \mathbf{T}_{\Omega_I}^{\mathrm{T}} \mathbf{M}_{\mu,\Omega_I} \mathbf{h}_{0,\Omega_I}, \quad (38)$$

where $\boldsymbol{\xi} = (\xi_k)$ is the vector of coefficients in (7). Note that the term $\jmath\, \omega\, \mathbf{T}_{\Omega_I}^{\mathrm{T}} \mathbf{M}_{\mu,\Omega_I} \mathbf{G}_{\Omega_I} \boldsymbol{\varphi}_{\Omega_I}$ is not considered again because it identically vanishes due to orthogonality (16).

D. COUPLED MATRIX SYSTEM

The continuity of magnetic fluxes and magnetic voltages across the interface Γ, with incidence matrices $\mathbf{G}_\Gamma$ (edges to nodes on $\mathcal{G}_\Gamma$) and $\widetilde{\mathbf{C}}_\Gamma = -\mathbf{G}_\Gamma^{\mathrm{T}}$ (faces to edges on $\widetilde{\mathcal{G}}_\Gamma$), is realized by the following transmission conditions:

$$\widetilde{\mathbf{C}}_\Gamma \widetilde{\mathbf{e}}_\Gamma + \jmath\, \omega\, \widetilde{\mathbf{b}}_\Gamma = \mathbf{0}, \quad (39)$$

$$\mathbf{h}_\Gamma = \mathbf{h}_{0,\Gamma} + \mathbf{G}_\Gamma \boldsymbol{\varphi}_\Gamma + \sum_{k=1}^{\beta_1} \xi_k\, \mathbf{t}_{\Gamma,k}, \quad (40)$$

where $\widetilde{\mathbf{e}}_\Gamma$ is the vector of electric voltages along dual edges of $\widetilde{\mathcal{G}}_\Gamma$, $\widetilde{\mathbf{b}}_\Gamma$ is the vector of magnetic fluxes through dual faces of $\widetilde{\mathcal{G}}_\Gamma$. Note that vectors of DOFs in (40), defined on $\mathcal{G}_\Gamma$, have similar meaning to corresponding terms in (7). Interface magnetic fluxes are obtained from (39) as $\widetilde{\mathbf{b}}_\Gamma = -(\jmath\, \omega)^{-1} \widetilde{\mathbf{C}}_\Gamma \widetilde{\mathbf{e}}_\Gamma$. Moreover, by noting that Γ and Γ_I have opposite orientation, it results $\widetilde{\mathbf{b}}_{\Gamma_I} = -\widetilde{\mathbf{b}}_\Gamma$. By putting interface fluxes in (34), the flux conservation equation in Ω_I becomes:

$$\jmath\, \omega\, \mathbf{G}_{\Omega_I}^{\mathrm{T}} \mathbf{M}_{\mu,\Omega_I} \mathbf{G}_{\Omega_I} \boldsymbol{\varphi}_{\Omega_I} - \widetilde{\mathbf{D}}_{\Omega_I \Gamma_I} \widetilde{\mathbf{C}}_\Gamma \widetilde{\mathbf{e}}_\Gamma = -\jmath\, \omega\, \mathbf{G}_{\Omega_I}^{\mathrm{T}} \mathbf{M}_{\mu,\Omega_I} \mathbf{h}_{0,\Omega_I}. \quad (41)$$

By noting that nodal and edge DOFs are continuous across Γ, variables of $\mathcal{G}_\Gamma$ in (40) are equal to the corresponding ones of $\mathcal{G}_{\Gamma_C}$ and $\mathcal{G}_{\Gamma_I}$. By the same reasoning as above, interface variables are derived from bulk ones by means of selection matrices, i.e., $\mathbf{h}_\Gamma = \widetilde{\mathbf{C}}^{\mathrm{T}}_{\Omega_C\Gamma_C}\mathbf{h}_{\Omega_C}$, $\mathbf{h}_{0,\Gamma} = \widetilde{\mathbf{C}}^{\mathrm{T}}_{\Omega_I\Gamma_I}\mathbf{h}_{0,\Omega_I}$, and $\boldsymbol{\varphi}_\Gamma = \widetilde{\mathbf{D}}^{\mathrm{T}}_{\Omega_I\Gamma_I}\boldsymbol{\varphi}_{\Omega_I}$. By letting the latter in (40), one obtains:

$$\widetilde{\mathbf{C}}^{\mathrm{T}}_{\Omega_C\Gamma_C}\mathbf{h}_{\Omega_C} - \mathbf{G}_\Gamma\widetilde{\mathbf{D}}^{\mathrm{T}}_{\Omega_I\Gamma_I}\boldsymbol{\varphi}_{\Omega_I} - \widetilde{\mathbf{C}}^{\mathrm{T}}_{\Omega_I\Gamma_I}\mathbf{T}_{\Omega_I}\boldsymbol{\xi} = \widetilde{\mathbf{C}}^{\mathrm{T}}_{\Omega_I\Gamma_I}\mathbf{h}_{0,\Omega_I}. \quad (42)$$

Due to DOFs continuity across the interface, $\widetilde{\mathbf{e}}_{\Gamma_C} = \widetilde{\mathbf{e}}_\Gamma$ holds in (31) and $\widetilde{\mathbf{e}}_{\Gamma_I} = \widetilde{\mathbf{e}}_\Gamma$ holds in (38). The final matrix system (43), as shown at the bottom of the page, yields to be complex symmetric and it is obtained by assembling together the diffusion equation (31), the topological constraints (38), the magnetostatic equation (41), and the transmission conditions (42). The system solution is unique after imposing the scalar potential in one node, arbitrarily chosen, for any connected component of Ω_I.

The final matrix system, in which electric voltages $\widetilde{\mathbf{e}}_\Gamma$ play the role of Lagrange multipliers, turns out to be in saddle–point form, so that a direct solver is typically needed for its solution. This can be expensive in terms of computational resources especially when real–sized 3–D eddy current problems are to be analyzed. Such multipliers can be eliminated from the matrix system adopting the following procedure.

By splitting $\mathbf{h}_{\Omega_I}$ into interface and non–interface DOFs, the following change of variables is obtained:

$$\mathbf{x} = \mathbf{P}\,\mathbf{x}^* + \mathbf{c}, \quad (44)$$

where:

$$\mathbf{x} = \left[\mathbf{h}_{\Omega_C},\ \boldsymbol{\varphi}_{\Omega_I},\ \boldsymbol{\xi}\right]^{\mathrm{T}},$$
$$\mathbf{x}^* = \left[\mathbf{h}_{\Omega_C\setminus\Gamma_C},\ \boldsymbol{\varphi}_{\Omega_I},\ \boldsymbol{\xi}\right]^{\mathrm{T}},$$
$$\mathbf{c} = \left[\widetilde{\mathbf{C}}_{\Omega_C\Gamma_C}\,\mathbf{h}_{0,\Gamma},\ \mathbf{0},\ \mathbf{0}\right]^{\mathrm{T}},$$

are column vectors. $\mathbf{h}_{\Omega_C\setminus\Gamma_C}$ is the vector of inner magnetic voltages of size $E_{\Omega_C\setminus\Gamma_C}$, i.e., the number of internal edges of $\mathcal{G}_{\Omega_C}$. The projection matrix in (44) is defined as:

$$\mathbf{P} = \begin{bmatrix} \mathbf{P}_{11} & \mathbf{P}_{12} & \mathbf{P}_{13} \\ \mathbf{0} & \mathbf{1}_{N_{\Omega_I}} & \mathbf{0} \\ \mathbf{0} & \mathbf{0} & \mathbf{1}_{\beta_1} \end{bmatrix}, \quad (45)$$

with blocks $\mathbf{P}_{11} = \mathbf{E}_{\Omega_C,\Omega_C\setminus\Gamma_C}$, $\mathbf{P}_{12} = \widetilde{\mathbf{C}}_{\Omega_C\Gamma_C}\mathbf{G}_\Gamma\widetilde{\mathbf{D}}^{\mathrm{T}}_{\Omega_I\Gamma_I}$, and $\mathbf{P}_{13} = \widetilde{\mathbf{C}}_{\Omega_C\Gamma_C}\widetilde{\mathbf{C}}^{\mathrm{T}}_{\Omega_I\Gamma_I}\mathbf{T}_{\Omega_I}$. $\mathbf{E}_{\Omega_C,\Omega_C\setminus\Gamma_C}$ is a selection matrix of size $E_{\Omega_C}\times E_{\Omega_C\setminus\Gamma_C}$. It is obtained from the identity matrix $\mathbf{1}_{E_{\Omega_C}}$, by deleting columns in correspondence of interface edges. Finally, $\mathbf{1}_{N_{\Omega_I}}$ and $\mathbf{1}_{\beta_1}$ are identity matrices of size N_{Ω_I}, i.e., the number of vertexes of $\mathcal{G}_{\Omega_I}$, and β_1.

The reduced system can be obtained after partitioning the original system (43) in the following way:

$$\begin{bmatrix} \mathbf{A} & \mathbf{B}^{\mathrm{T}} \\ \mathbf{B} & \mathbf{0} \end{bmatrix}\begin{bmatrix} \mathbf{x} \\ \widetilde{\mathbf{e}}_\Gamma \end{bmatrix} = \begin{bmatrix} \mathbf{b} \\ \widetilde{\mathbf{C}}^{\mathrm{T}}_{\Omega_I\Gamma_I}\mathbf{h}_{0,\Omega_I} \end{bmatrix}, \quad (46)$$

where matrix $\mathbf{A}$ is the upper 3×3 square block in (43) and

$$\mathbf{B} = \left[\widetilde{\mathbf{C}}^{\mathrm{T}}_{\Omega_C\Gamma_C}, -\mathbf{G}_\Gamma\widetilde{\mathbf{D}}^{\mathrm{T}}_{\Omega_I\Gamma_I}, -\widetilde{\mathbf{C}}^{\mathrm{T}}_{\Omega_I\Gamma_I}\mathbf{T}_{\Omega_I}\right],$$
$$\mathbf{b} = \left[\mathbf{0}, -\jmath\omega\mathbf{G}^{\mathrm{T}}_{\Omega_I}\mathbf{M}_{\mu,\Omega_I}\mathbf{h}_{0,\Omega_I}, -\jmath\omega\mathbf{T}^{\mathrm{T}}_{\Omega_I}\mathbf{M}_{\mu,\Omega_I}\mathbf{h}_{0,\Omega_I}\right]^{\mathrm{T}}.$$

From $\widetilde{\mathbf{C}}^{\mathrm{T}}_{\Omega_C\Gamma_C}\mathbf{E}_{\Omega_C,\Omega_C\setminus\Gamma} = \mathbf{0}$, $\widetilde{\mathbf{C}}^{\mathrm{T}}_{\Omega_C\Gamma_C}\widetilde{\mathbf{C}}_{\Omega_C\Gamma_C} = \mathbf{1}$, it results

$$\mathbf{B}\,\mathbf{P} = \widetilde{\mathbf{C}}^{\mathrm{T}}_{\Omega_C\Gamma_C}[\mathbf{P}_{11}, \mathbf{P}_{12}, \mathbf{P}_{13}] - \left[\mathbf{0}, \mathbf{G}_\Gamma\widetilde{\mathbf{D}}^{\mathrm{T}}_{\Omega_I\Gamma_I}, \widetilde{\mathbf{C}}^{\mathrm{T}}_{\Omega_I\Gamma_I}\mathbf{T}_{\Omega_I}\right] = \mathbf{0}. \quad (47)$$

Therefore, transmission conditions, which correspond to the lower row in (46), can be equivalently enforced by:

$$\mathbf{B}\,\mathbf{x} = \mathbf{B}\mathbf{P}\,\mathbf{x}^* + \mathbf{B}\,\mathbf{c} = \widetilde{\mathbf{C}}^{\mathrm{T}}_{\Omega_I\Gamma_I}\mathbf{h}_{0,\Omega_I}. \quad (48)$$

By noting that $\mathbf{P}^{\mathrm{T}}\mathbf{B}^{\mathrm{T}} = \mathbf{0}$, which is the transpose of (47), the upper row of (46) provides the final reduced matrix system:

$$\mathbf{P}^{\mathrm{T}}\mathbf{A}\mathbf{P}\,\mathbf{x}^* = \mathbf{P}^{\mathrm{T}}\mathbf{b} - \mathbf{P}^{\mathrm{T}}\mathbf{A}\mathbf{c}. \quad (49)$$

It can be easily observed, by simple inspection, that $\mathbf{P}$ is a full rank matrix. Therefore, the reduced system is also full rank and complex symmetric such as (43). The key advantage with respect to system (43) is that (49) can be solved by an iterative solver such as TFQMR with SSOR preconditioning, with much less computational effort compared to a direct LU solver needed for (43) in a saddle–point form. It has also been verified by numerical tests that other solvers, such as COCG or BiCGSTAB, show comparable performance.

VI. NUMERICAL RESULTS

The **h–φ** formulation for multiply connected domains is implemented in MATLAB® software environment with vectorized functions in order to optimize computational time for the matrix assembly process. The numerical code is first tested by considering a benchmark with axisymmetric model geometry in order to assess the accuracy of 3–D CM formulation against a reference third-order 2-D FEM solution. The code applicability to more general 3-D eddy current problems is validated by considering the TEAM Problem 3 "Bath Plate" model, involving a thin aluminum plate with two holes and excited by an AC current–driven coil [37]. All

$$\begin{bmatrix} \mathbf{C}^{\mathrm{T}}_{\Omega_C}\mathbf{M}_{\rho,\Omega_C}\mathbf{C}_{\Omega_C} + \jmath\omega\mathbf{M}_{\mu,\Omega_C} & \mathbf{0} & \mathbf{0} & \widetilde{\mathbf{C}}_{\Omega_C\Gamma_C} \\ \mathbf{0} & \jmath\omega\mathbf{G}^{\mathrm{T}}_{\Omega_I}\mathbf{M}_{\mu,\Omega_I}\mathbf{G}_{\Omega_I} & \mathbf{0} & -\widetilde{\mathbf{D}}_{\Omega_I\Gamma_I}\mathbf{G}^{\mathrm{T}}_\Gamma \\ \mathbf{0} & \mathbf{0} & \jmath\omega\mathbf{T}^{\mathrm{T}}_{\Omega_I}\mathbf{M}_{\mu,\Omega_I}\mathbf{T}_{\Omega_I} & -\mathbf{T}^{\mathrm{T}}_{\Omega_I}\widetilde{\mathbf{C}}_{\Omega_I\Gamma_I} \\ \widetilde{\mathbf{C}}^{\mathrm{T}}_{\Omega_C\Gamma_C} & -\mathbf{G}_\Gamma\widetilde{\mathbf{D}}^{\mathrm{T}}_{\Omega_I\Gamma_I} & -\widetilde{\mathbf{C}}^{\mathrm{T}}_{\Omega_I\Gamma_I}\mathbf{T}_{\Omega_I} & \mathbf{0} \end{bmatrix}\begin{bmatrix} \mathbf{h}_{\Omega_C} \\ \boldsymbol{\varphi}_{\Omega_I} \\ \boldsymbol{\xi} \\ \widetilde{\mathbf{e}}_\Gamma \end{bmatrix} = \begin{bmatrix} \mathbf{0} \\ -\jmath\omega\mathbf{G}^{\mathrm{T}}_{\Omega_I}\mathbf{M}_{\mu,\Omega_I}\mathbf{h}_{0,\Omega_I} \\ -\jmath\omega\mathbf{T}^{\mathrm{T}}_{\Omega_I}\mathbf{M}_{\mu,\Omega_I}\mathbf{h}_{0,\Omega_I} \\ \widetilde{\mathbf{C}}^{\mathrm{T}}_{\Omega_I\Gamma_I}\mathbf{h}_{0,\Omega_I} \end{bmatrix} \quad (43)$$

numerical analyses reported below are run on a laptop with an Intel Core i7-6920HQ processor (2.9 GHz clock).

A. AXISYMMETRIC INDUCTOR

In order to get highly accurate results for comparisons, a 2–D FEM axisymmetric model discretized by third–order element is considered. Fig. 3 shows the benchmark model, in which coordinates are given with respect to a cylindrical reference frame (r, z). A multiply connected conducting shell Ω_C (5 mm inner radius, 5 mm thick, 4 cm long, $\mu_r = 2$ relative magnetic permeability, $\sigma = 25$ MS/m conductivity, centered at $r = 75$ mm, $z = 0$ mm) with two air cavities (square cross–section, 2 mm side, centered at $r = 75$ mm, $z = \pm 30$ mm) is excited by an AC current–driven coil Ω_0 ($J_0 = 10^6$ A/m current density, 200 Hz frequency, square cross–section, 4 mm side, centered at $r = 150$ mm, $z = 0$ mm). The air domain Ω_I is a rectangular box (300 mm width, 800 mm height, $\mu_r = 1$ permeability, centered at $r = 150$ mm, $z = 0$ mm) enclosing the whole geometry. 2–D FEM model is meshed into 24 714 third–order triangles and 12 578 vertexes, after refining till convergence. Its solution in the whole domain (real and imaginary parts of r–, z–axis components H_r, H_z) is used in order to estimate the accuracy of the 3–D CM model implementing the **h**–φ formulation. The solution for 3–D CM is evaluated for different mesh sizes (reported in Table 1) in order to assess the convergence properties of the model. The mesh size h is defined as the maximum diameter of spheres circumscribing mesh tetrahedrons.

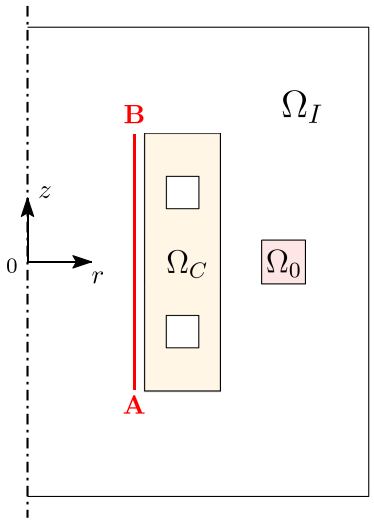

FIGURE 3. Axisymmetric inductor model used for 2-D FEM validations: Ω_C is the multiply connected conducting subdomain, Ω_I is the air subdomain, Ω_0 is the coil subdomain. Magnetic field is computed along line A–B (in red).

The magnetic field distribution in the air region is first compared along a vertical line A–B, with coordinates $r = 4$ mm, $z = [-20, 20]$ mm (depicted in red in Fig. 3). For 3–D CM, the full model geometry, obtained by revolving the 2–D model of Fig. 3 with respect to the z–axis, is considered. This model is first discretized into 195 536 tetrahedrons (where 186 240 elements are used for the air domain), 394 650 faces, 233 704 edges, and 34 591 vertexes. This corresponds to the coarsest mesh refinement in Table 1 ($h = 2.7$ mm). By inspecting the model topology in Fig. 3 it can be observed that $\beta_1 = 3$; therefore, three loop fields are expected to be extracted by Algorithm 1. The source field $\mathbf{h}_{0,\Omega_I}$ is generated, according to the procedure described in Section V-A, in 0.70 s CPU time (where LSMR solver for rectangular systems (22) and (17) is set to 10^{-12} tolerance). A topological matrix $\mathbf{T}_{\Omega_I}$ of size 224 931 $\times$ 3 is generated by Algorithm 1 in 3.24 s CPU time (with the same tolerance as above for both LSMR and AGMG solvers). The final system (49), consisting of 42 524 DOFs, is solved by TFQMR, with SSOR preconditioning, in 3.18 s. Fig. 4 shows that, for the model with $h = 2.7$ mm, the solver attains 10^{-10} tolerance in about 350 iterations, with a smooth convergence pattern. The z–axis magnetic field component is evaluated along the vertical line by 3–D CM on 401 equally spaced points and compared to the corresponding 2–D FEM results (Fig. 5). The maximum discrepancies from 2–D FEM, for the real and imaginary parts of H_z, are 6.93% and 7.13%, respectively.

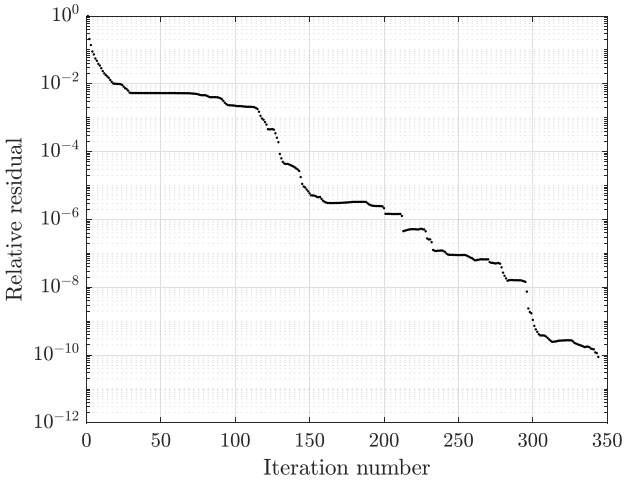

FIGURE 4. Convergence path of the TFQMR solver with SSOR preconditioning for the coarsest mesh refinement ($h = 2.7$ mm).

In order to assess the convergence properties of **h**–φ formulation, the magnetic field distributions of 2–D FEM (**H**, taken to be as the exact solution) and 3–D CM ($\mathbf{H}_h$, depending on the mesh size) are compared in the whole computational domain. The 3–D CM accuracy is estimated in terms of L^2–norm in Ω, as:

$$e_H = \frac{\|\mathbf{H}_h - \mathbf{H}\|_{L^2(\Omega)}}{\|\mathbf{H}\|_{L^2(\Omega)}}. \tag{50}$$

It can be observed in Table 1 that CPU time required for both topological basis construction and matrix system solution is limited even for meshes of several millions of elements. Fig. 6 shows that the **h**–φ formulation has a linear convergence behavior with respect to the L^2–norm, which is the same of the more classical **A**–**A** formulation (see, e.g., convergence

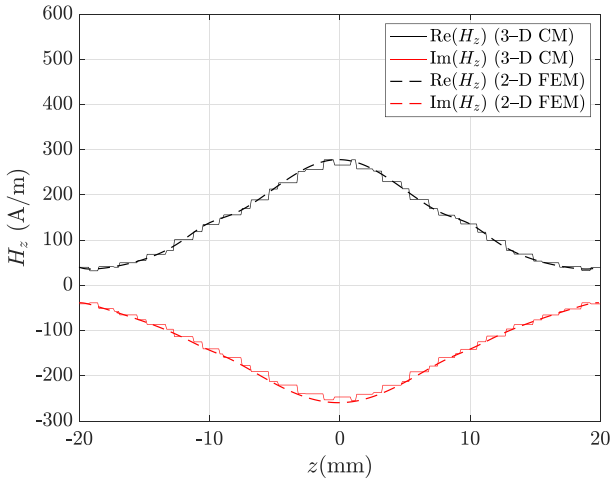

FIGURE 5. Real and imaginary parts of the z-axis magnetic field component along line a–b in Fig. 3 ($x = 4$ mm, $y = 0$, $z = [-20, 20]$ mm, $h = 2.7$ mm; 3-D CM plot is in straight line, 2-D FEM plot is in dashed line).

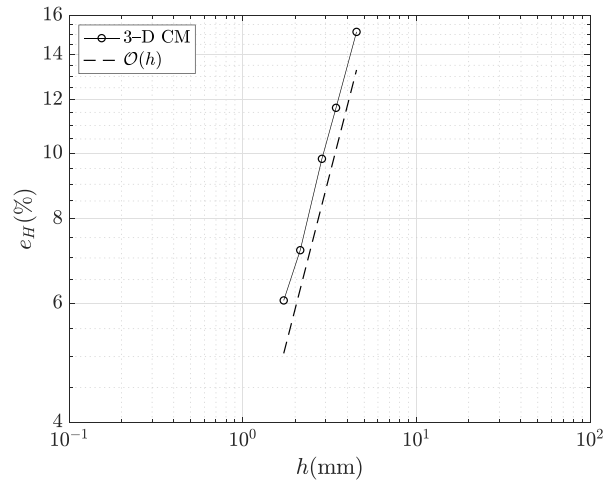

FIGURE 6. Discrepancy (L^2–norm) in Ω between the magnetic field computed by 2-D FEM (third order) and by 3-D CM formulation (dashed line expresses theoretical first–order convergence).

plots in [25]). The discrepancy values in Fig. 6 are computed by (50), for each mesh size given in Table 1.

B. TEAM PROBLEM 3: "BATH PLATE"

The **h**–φ method is validated against the so–called "Bath Plate"' problem, i.e., a benchmark proposed in the literature for 3–D time–harmonic magnetic formulations [37]. This problem consists in a conducting plate (32.78 MS/m electrical conductivity, $\mu_r = 1$ relative magnetic permeability, 6.35 mm thick, 60 mm wide, 110 mm long) excited by an AC current–driven cylindrical coil (1240 A turn, 20 mm inner radius, 40 mm outer radius, 20 mm thick, located 15 mm above the plate) at two different frequency values (50 Hz, 200 Hz). Two holes with square cross-section (40 mm side) are symmetrically placed with respect to the (x, z) vertical plane, so that the conducting domain Ω_C turns out to be

TABLE 1. Computational Requirements For Generating Topological Fields and Solving the Final Matrix System (SSOR + TFQMR iterative solver).

h (mm)	# tets	# DOFs	CPU time (s) (generators)	CPU time (s) (solver)
2.7	195 536	42 524	3.24	3.18
2.0	473 426	97 700	10.26	8.45
1.6	931 811	190 000	23.81	22.99
1.2	2 234 193	462 389	83.71	83.33
1.0	3 871 177	797 512	130.86	175.56

multiply connected. The origin of the Cartesian reference frame (x, y, z) is centered on the plate surface; the coil vertical axis is the z–axis. The whole model is placed inside a bounding box (200 mm side cube) on the boundary of which a null magnetic flux condition is applied.

To examine the accuracy of 3-D CM results, the real and imaginary parts of the z–component of the magnetic flux density are computed, for both frequency values, along a line A–B, which is located 0.5 mm above the plate surface on the (y, z) symmetry plane. The coordinates of line A–B are: $x = 0$ mm, $y = [-55, 55]$ mm, $z = 0.5$ mm. Fig. 7 shows the tetrahedral mesh used by the 3-D CM for discretizing the coil and conducting domains and the field calculation line (depicted in blue). By inspecting the model topology in Fig. 7 it can be observed that $\beta_1 = 2$; therefore, two loop fields are expected to be generated by Algorithm 1. For the sake of comparison, numerical results from a 3–D FEM commercial software package, implementing a classical **A**–**A** formulation, are used. For 3–D CM, the whole domain is discretized into 213 640 tetrahedrons (154 635 elements for the conducting plate, 3 541 elements for the coil, and 154 635 for the air domain), with $h = 6.21$ mm mesh size. In particular, mesh is refined in the conducting plate in order to capture the skin effect with good accuracy ($h = 1.61$ mm in Ω_C, which is much smaller than the skin depth at 200 Hz, i.e., 6.22 mm). In order to get a reference solution, the 3–D FEM discretization is refined up to convergence (182 862 second–order tetrahedrons are used; only a half of the problem is considered due to symmetry). **A**–**A** formulation needs to introduce a fake conductivity in the air region (0.1 S/m) for the stabilization of the final matrix system. This correction, which is not required by the **h**–φ method, introduces an approximation in the numerical results. 3–D FEM model, consisting of 1 165 824 DOFs, is solved by TFQMR solver with multigrid preconditioning in 161 s CPU time to attain a 10^{-10} tolerance. Pre–processing of CM encompasses the computation of source field (0.75 s CPU time) and topological matrix (188 576 × 2 size, 4.82 s CPU time), with both LSMR and AGMG tolerances set to 10^{-12}. The iterative solution by TFQMR + SSOR solver of the reduced final system (with 89 997 DOFs) requires 18.63 s CPU time, with 813 iterations, to attain 10^{-10} tolerance.

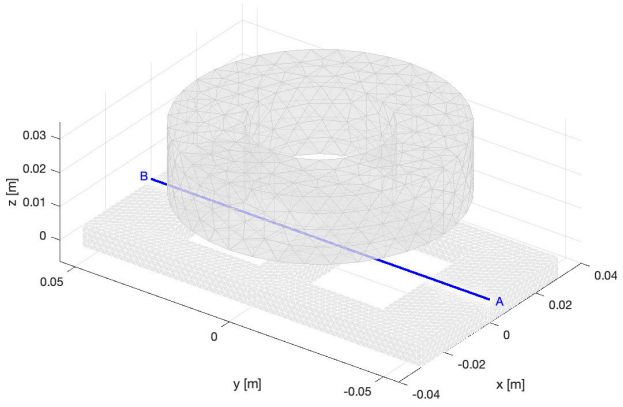

FIGURE 7. Tetrahedral mesh of the Team 3 model used by the **h**–φ method in the numerical simulation (field calculation line A-B is depicted in blue; for the sake of clarity, only coil and conducting domain meshes have been plotted).

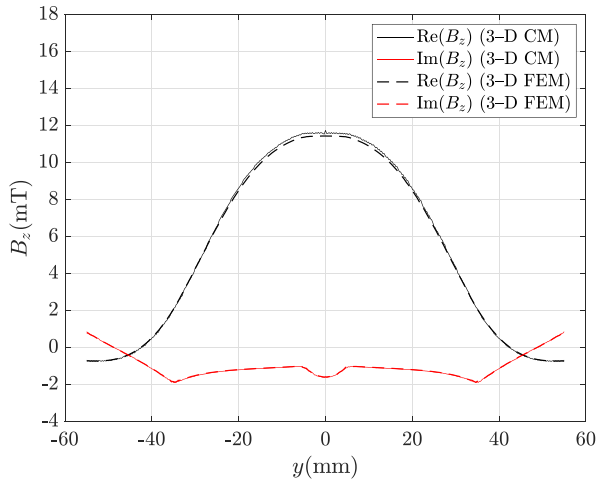

FIGURE 8. Real and imaginary parts of the z-axis magnetic flux density component at 50 Hz along line A–B in Fig. 7 ($x = 0$ mm, $y = [-55, 55]$ mm, $z = 0.5$ mm; 3-D CM plot is in straight line, 3-D FEM plot is in dashed line).

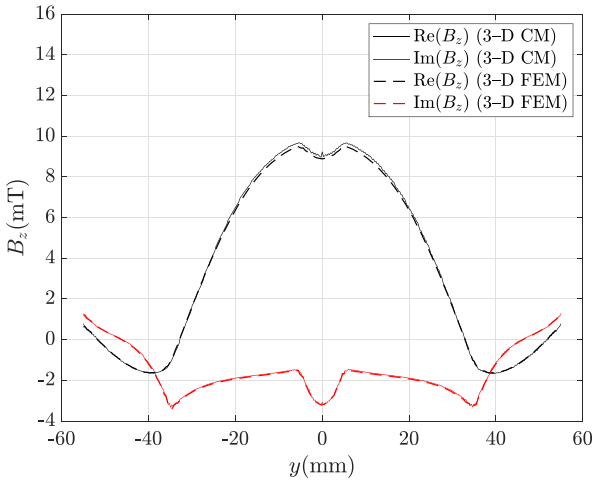

FIGURE 9. Real and imaginary parts of the z-axis magnetic flux density component at 200 Hz along line A–B in Fig. 7 ($x = 0$ mm, $y = [-55, 55]$ mm, $z = 0.5$ mm; 3-D CM plot is in straight line, 3-D FEM plot is in dashed line).

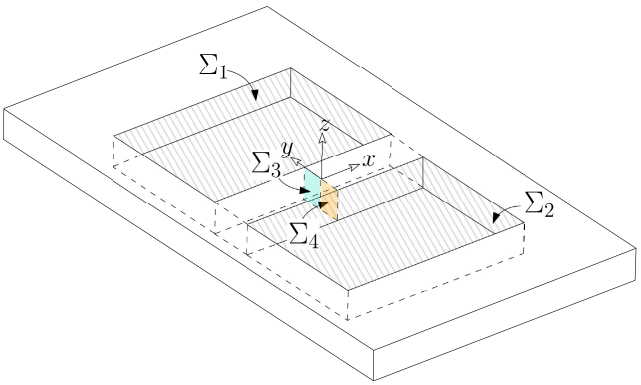

FIGURE 10. Cut surfaces used for determining global quantities indicated by the Team 3 problem (Σ_1, Σ_2 for magnetic fluxes; Σ_3, Σ_4 for eddy currents).

TABLE 2. Real and imaginary parts of magnetic flux (μ Wb) computed through surfaces Σ_1, Σ_2 by 3–D CM and 3–D FEM at 50 Hz and 200 Hz.

		$Re(b_{\Sigma_1})$	$Im(b_{\Sigma_1})$	$Re(b_{\Sigma_2})$	$Im(b_{\Sigma_2})$
50 Hz	CM	8.15	−1.90	7.98	−1.85
	FEM	7.84	−1.89	7.84	−1.89
200 Hz	CM	4.82	−3.04	4.73	−2.93
	FEM	4.49	−3.10	4.49	−3.10

The z–axis magnetic flux density component is evaluated along the horizontal line A–B by 3–D CM on 401 equally spaced points and compared to the corresponding 3–D FEM results (Fig. 8, 50 Hz, and Fig. 9, 200 Hz). The maximum discrepancies from 3–D FEM, for the real and imaginary parts of B_z are, respectively, 2.68% and 5.02%, at 50 Hz, and 3.63% and 5.89%, at 200 Hz. Therefore, even by using a relatively coarse mesh refinement for 3–D CM, a good agreement with second–order FEM is obtained.

The global quantities to be determined according to Team 3 problem are magnetic fluxes trough the plate holes and eddy currents trough the central limb. Magnetic fluxes $b_{\Sigma_1}, b_{\Sigma_2}$ are computed by both 3–D CM and second-order FEM through the same horizontal surfaces on the plane $z = 0$: Σ_1, with coordinates $x = [-20, 20]$ mm, $y = [5, 35]$ mm, and Σ_2, with coordinates $x = [-20, 20]$ mm, $y = [-35, -5]$ mm (Fig. 10). Eddy current phasors $I_{\Sigma_3}, I_{\Sigma_4}$ are computed through the same vertical surfaces on the plane $x = 0$: Σ_3, with coordinates $y = [0, 5]$ mm, $z = [-6.35, 0]$ mm, and Σ_4, with coordinates $y = [-5, 0]$ mm, $z = [-6.35, 0]$ mm. Due to model symmetry, relationships $b_{\Sigma_1} = b_{\Sigma_2}$, and $I_{\Sigma_3} = -I_{\Sigma_4}$ theoretically hold. Table 2 shows that real and imaginary parts of magnetic fluxes through Σ_1 and Σ_2, computed by 3–D CM, are in good agreement with reference values obtained with second–order FEM at 50 Hz and 200 Hz.

TABLE 3. Real and imaginary parts of eddy current (A) computed through surfaces Σ_3, Σ_4 by 3–D CM and 3–D FEM at 50 Hz and 200 Hz.

		$Re(I_{\Sigma_3})$	$Im(I_{\Sigma_3})$	$Re(I_{\Sigma_4})$	$Im(I_{\Sigma_4})$
50 Hz	CM	1.41	7.63	−1.40	−7.60
	FEM	1.37	7.54	−1.37	−7.54
200 Hz	CM	11.10	21.49	−11.04	−21.42
	FEM	10.88	21.34	−10.88	−21.34

Similar considerations apply to eddy current values through surfaces Σ_3 and Σ_4, reported in Table 3, which are obtained for the same frequency values.

VII. CONCLUSION

A novel **h**–$\boldsymbol{\varphi}$ formulation for solving 3–D time–harmonic eddy–current problems in multiply connected bounded domains has been presented. Its main advantage is that, after the introduction of cohomology generators, nodal variables can be used for the discretization of insulating domains. The Algorithm 1 provides a maximal set of generators with limited computational time even with millions of elements in the mesh. The approach presented in [12] has been extended to the case of coils with prescribed analytical current density. A procedure for eliminating Lagrange multipliers, required for transmission conditions, has been proposed. It makes it possible to obtain a complex symmetric system, with lower number of DOFs, amenable to iterative solution. Numerical experiments have shown that the **h**–$\boldsymbol{\varphi}$ method is both accurate, since it attains first–order convergence in L^2–norm, and efficient, since real–sized 3–D models with millions of mesh elements are analyzed in a few minutes on a standard laptop.

REFERENCES

[1] O. Bíró, K. Preis, W. Renhart, K. R. Richter, and G. Vrisk, "Performance of different vector potential formulations in solving multiply connected 3-D eddy current problems," *IEEE Trans. Magn.*, vol. 26, no. 2, pp. 438–441, Mar. 1990.

[2] O. Bíró, "Edge element formulations of eddy current problems," *Comput. Methods Appl. Mech. Eng.*, vol. 169, nos. 3–4, pp. 391–405, Feb. 1999.

[3] Z. Ren, "T–Ω formulation for eddy-current problems in multiply connected regions," *IEEE Trans. Magn.*, vol. 38, no. 2, pp. 557–560, Mar. 2002.

[4] L. Kettunen, K. Forsman, and A. Bossavit, "Formulation of the eddy current problem in multiply connected regions in terms of H," *Int. J. Numer. Meth. Engng.*, vol. 41, pp. 935–954, 1998.

[5] L. Kettunen, K. Forsman, and A. Bossavit, "Discrete spaces for DIV and curl-free fields," *IEEE Trans. Magn.*, vol. 34, no. 5, pp. 2551–2554, Sep. 1998.

[6] M. Pellikka, S. Suuriniemi, L. Kettunen, and C. Geuzaine, "Homology and cohomology computation in finite element modeling," *SIAM J. Sci. Comput.*, vol. 35, no. 5, pp. B1195–B1214, Jan. 2013.

[7] S. Peltier, S. Alayrangues, L. Fuchs, and J.-O. Lachaud, "Computation of homology groups and generators," *Comput. Graph.*, vol. 30, no. 1, pp. 62–69, Feb. 2006.

[8] F. Henrotte and K. Hameyer, "An algorithm to construct the discrete cohomology basis functions required for magnetic scalar potential formulations without cuts," *IEEE Trans. Magn.*, vol. 39, no. 3, pp. 1167–1170, May 2003.

[9] P. Zhou, Z. Badics, D. Lin, and Z. J. Cendes, "Nonlinear T-Ω formulation including motion for multiply connected 3-D problems," *IEEE Trans. Magn.*, vol. 44, no. 6, pp. 718–721, Jun. 2008.

[10] P. Dłotko, R. Specogna, and F. Trevisan, "Automatic generation of cuts on large-sized meshes for the T–Ω geometric eddy-current formulation," *Comput. Methods Appl. Mech. Eng.*, vol. 198, nos. 47–48, pp. 3765–3781, Oct. 2009.

[11] P. Dłotko and R. Specogna, "Physics inspired algorithms for (co)homology computations of three-dimensional combinatorial manifolds with boundary," *Comput. Phys. Commun.*, vol. 184, no. 10, pp. 2257–2266, Oct. 2013.

[12] F. Moro and L. Codecasa, "Enforcing lumped parameter excitations in edge-element formulations by using a fast iterative approach," *IEEE Trans. Magn.*, vol. 56, no. 1, pp. 1–4, Jan. 2020, Art. no. 7502604.

[13] A. Bossavit, "Two dual formulations of the 3-D eddy–currents problem," *COMPEL*, vol. 4, no. 2, pp. 105–116, 1985.

[14] J. van Welij, "Calculation of eddy currents in terms of H on hexahedra," *IEEE Trans. Magn.*, vol. 21, no. 6, pp. 2239–2241, Nov. 1985.

[15] J. P. Webb and B. Forghani, "The low-frequency performance of H-Φ and T-Ω methods using edge elements for 3D eddy current problems," *IEEE Trans. Magn.*, vol. 29, no. 6, pp. 2461–2463, Nov. 1993.

[16] P. Dular, C. Geuzaine, and W. Legros, "A natural method for coupling magnetodynamic H-formulations and circuit equations," *IEEE Trans. Magn.*, vol. 35, no. 3, pp. 1626–1629, May 1999.

[17] A. Bermúdez, R. Rodríguez, and P. Salgado, "Numerical solution of eddy current problems in bounded domains using realistic boundary conditions," *Comput. Methods Appl. Mech. Eng.*, vol. 194, nos. 2–5, pp. 411–426, Feb. 2005.

[18] A. Alonso Rodríguez, E. Bertolazzi, R. Ghiloni, and A. Valli, "Finite element simulation of eddy current problems using magnetic scalar potentials," *J. Comput. Phys.*, vol. 294, pp. 503–523, Aug. 2015.

[19] J. Smajic, "A novel variant of the H–Φ field formulation for magnetostatic and eddy current problems," *COMPEL-Int. J. Comput. Math. Electr. Electron. Eng.*, vol. 38, no. 5, pp. 1545–1561, Sep. 2019.

[20] D. Casati, J. Smajic, and R. Hiptmair, "H–Φ field formulation with lumped sources and unbounded domains," *IEEE Trans. Magn.*, vol. 56, no. 1, pp. 1–4, Jan. 2020, Art. no. 7501404.

[21] E. Tonti, "Why starting from differential equations for computational physics?" *J. Comput. Phys.*, vol. 257, pp. 1260–1290, Jan. 2014.

[22] L. Codecasa, "Refoundation of the Cell Method using augmented dual grids," *IEEE Trans. Magn.*, vol. 50, no. 2, pp. 1–4, Feb. 2014, Art. no. 7012204.

[23] P. Alotto, M. Bullo, M. Guarnieri, and F. Moro, "A coupled thermo-electromagnetic formulation based on the cell method," *IEEE Trans. Magn.*, vol. 44, no. 6, pp. 702–705, Jun. 2008.

[24] P. Alotto, G. Gruosso, F. Moro, and M. Repetto, "A boundary integral formulation for eddy current problems based on the cell method," *IEEE Trans. Magn.*, vol. 44, no. 6, pp. 770–773, Jun. 2008.

[25] F. Moro and L. Codecasa, "A 3-D hybrid cell boundary element method for time-harmonic eddy current problems on multiply connected domains," *IEEE Trans. Magn.*, vol. 55, no. 3, pp. 1–11, Mar. 2019, Art. no. 9200111.

[26] A. A. Rodríguez, E. Bertolazzi, R. Ghiloni, and A. Valli, "Construction of a finite element basis of the first de rham cohomology group and numerical solution of 3D magnetostatic problems," *SIAM J. Numer. Anal.*, vol. 51, no. 4, pp. 2380–2402, Jan. 2013.

[27] I. Mayergoyz, "A new approach to the calculation of three-dimensional skin effect problems," *IEEE Trans. Magn.*, vol. 19, no. 5, pp. 2198–2200, Sep. 1983.

[28] A. Bossavit, *Computational Electromagnetism: Variational Formulations, Complementarity, Edge Elements*. New York, NY, USA: Academic, 1998.

[29] A. Bossavit and L. Kettunen, "Yee-like schemes on staggered cellular grids: A synthesis between FIT and FEM approaches," *IEEE Trans. Magn.*, vol. 36, no. 4, pp. 861–867, Jul. 2000.

[30] A. G. Kladas and J. A. Tegopoulos, "A new scalar potential formulation for 3-D magnetostatics necessitating no source field calculation," *IEEE Trans. Magn.*, vol. 28, no. 2, pp. 1103–1106, Mar. 1992.

[31] A. G. Kladas and J. A. Tegopoulos, "3D eddy currents modelling by means of a particular reduced scalar potential technique," *IEEE Trans. Magn.*, vol. 33, no. 2, pp. 1350–1353, Mar. 1997.

[32] Z. Ren, "Influence of the RHS on the convergence behaviour of the curl-curl equation," *IEEE Trans. Magn.*, vol. 32, no. 3, pp. 655–658, May 1996.

[33] K. Preis, I. Bardi, O. Biro, C. Magele, G. Vrisk, and K. R. Richter, "Different finite element formulations of 3D magnetostatic fields," *IEEE Trans. Magn.*, vol. 28, no. 2, pp. 1056–1059, Mar. 1992.

[34] L. Codecasa, V. Minerva, and M. Politi, "Use of barycentric dual grids for the solution of frequency domain problems by FIT," *IEEE Trans. Magn.*, vol. 40, no. 2, pp. 1414–1419, Mar. 2004.
[35] A. Napov and Y. Notay, "An algebraic multigrid method with guaranteed convergence rate," *SIAM J. Sci. Comput.*, vol. 34, no. 2, pp. 1079–1109, 2012.
[36] G. H. Golub and C. F. Van Loan, *Matrix Computations*. Baltimore, MD, USA: The Johns Hopkins Univ. Press, 2013.
[37] D. Rodger, "Benchmark problem 3 (the bath plate)," *COMPEL*, vol. 7, nos. 1–2, pp. 47–63, 1988.

FEDERICO MORO (Member, IEEE) received the B.S. degree in mathematics, the M.S. degree in electrical engineering, and the Ph.D. degree in bioelectromagnetic and electromagnetic compatibility from the University of Padova, Italy, in 2003, 2007, and 2012, respectively.

From 2007 to 2010, he was a Research Associate with the Department of Electrical Engineering, University of Padova. Since 2010, he has been an Assistant Professor of electrical engineering with the Department of Industrial Engineering, University of Padova. He is the author of more than 100 articles in peer-reviewed international journals and conference proceedings. His research interests include numerical methods for computing electromagnetic problems and the numerical modeling of multiphysics and multiscale problems.

JASMIN SMAJIC (Senior Member, IEEE) received the B.Sc. degree from the Faculty of Electrical Engineering, Tuzla, Bosnia and Herzegovina, in 1996, and the M.Sc. and Ph.D. degrees from the Faculty of Electrical Engineering and Computing, Zagreb, Croatia, in 1998 and 2001, respectively. From 2002 to 2004, he was a Postdoctoral Research Fellow with the Computational Optics group of the Laboratory for Electromagnetic Fields and Microwave Electronics, Swiss Federal Institute of Technology (ETH Zürich), Switzerland. From 2004 to 2011, he was a Scientist with the ABB Corporate Research Centre, Baden-Dättwil, Switzerland. His work in ABB covered a wide range of projects in the field of computational electromagnetics for developing new power technologies and products. At ETH Zürich, he has been teaching at the master's and Ph.D. level several courses on computational electromagnetics and physical modeling since 2007. Since 2011, he has also been a Professor of electrical engineering with the University of Applied Sciences in Rapperswil, Switzerland, where he is currently leading the Computational and Applied Electromagnetics Group. He has authored over 100 scientific publications and dozens of patents. He is also a member of CIGRE.

LORENZO CODECASA (Member, IEEE) received the Ph.D. degree in electronic engineering from the Politecnico di Milano, in 2001.

From 2002 to 2010, he worked as an Assistant Professor of electrical engineering with the Department of Electronics, Information, and Bioengineering, Politecnico di Milano. Since 2010, he has been worked as an Associate Professor of electrical engineering with the Politecnico di Milano. His research interests include theoretical analysis and in the computational investigation of electric circuits and electromagnetic fields. In his research on heat transfer and thermal management of electronic components, he has introduced original industrial-strength approaches to the extraction of compact thermal models, currently available in market leading commercial software. In his research areas, he has authored or coauthored over 200 articles in refereed international journals and conference proceedings. For these activities, in 2016, he received the Harvey Rosten Award for Excellence. He has been serving as an Associate Editor for the IEEE TRANSACTIONS OF COMPONENTS, PACKAGING AND MANUFACTURING TECHNOLOGY. He has also been serving as a Chair for the Conference Thermal Investigation of Integrated Circuits (THERMINIC).